Polymer 50 (2009) 5124–5133

Contents lists available at ScienceDirect

Polymer

journal homepage: www.elsevier.com/locate/polymer

New polypropylene blends toughened by polypropylene/poly(ethylene-*co*-propylene) in-reactor alloy: Compositional and morphological influence on mechanical properties

Rongbo Li [a,b], Xiuqin Zhang [a], Ying Zhao [a], Xuteng Hu [c], Xutao Zhao [c], Dujin Wang [a,*]

[a] Beijing National Laboratory for Molecular Sciences, CAS Key Laboratory of Engineering Plastics, Institute of Chemistry, Chinese Academy of Sciences, Beijing 100190, China
[b] Graduate School of Chinese Academy of Sciences, Beijing 100190, China
[c] PetroChina Petrochemical Research Institute, Beijing 100083, China

ARTICLE INFO

Article history:
Received 12 June 2009
Accepted 6 September 2009
Available online 12 September 2009

Keywords:
Polypropylene blends
Polypropylene/poly(ethylene-*co*-propylene) in-reactor alloy
Structure-property correlation

ABSTRACT

A new toughening agent, polypropylene/poly(ethylene-*co*-propylene) in-reactor alloy (EP-P), has been adopted to modify isotactic polypropylene (PP) in present study. Systematic investigation has been performed on the inter-compositional interaction, crystalline structure, and phase morphology of a series of PP/EP-P blends. It has been found that the PP component from EP-P is thoroughly miscible with neat PP and they together serve as the matrix of the PP/EP-P blends, while the ethylene–propylene random copolymers (EPR) act as the dispersed phase. The ethylene–propylene segmented copolymers (EPS), behaving as the compatibilizer between the EPR dispersed phase and PP matrix, strengthen mutual incorporation and effective diffusion of the amorphous PP segments and the EPR molecules. Based on the in-depth understanding of the crystalline structure and phase morphology, the correlation between morphological structure and mechanical properties has been established. The excellent impact toughness of PP/EP-P blends with higher EP-P content is mainly attributed to the small PP crystallites scattered in the blends and the well dispersed EP copolymer domains in PP matrix.

1. Introduction

Isotactic polypropylene (PP), as one of the most important thermoplastics, has been widely used in various industrial fields such as automotive parts, furniture, and packages. However, the application of PP as high-performance engineering plastic is limited by its poor impact toughness, in particular at low temperatures. In the past three decades, the impact strength of PP has been improved by blending it with multiple elastomers such as ethylene–propylene random copolymer (EPR) [1–4], ethylene–propylene–diene terpolymer (EPDM) [5–8], styrene–ethylene/butylene–styrene triblock copolymer (SEBS) [9], and polypropylene-*block*-poly(ethylene–propylene) copolymer (PP-*co*-EP) [10], etc. The advances in the studies of toughening methods and theories interpreting toughening mechanisms of PP/elastomer blends have been also reviewed [11]. Though numerous achievements have been realized in the research area of elastomer toughening PP, the modified mechanical properties of these blending systems cannot fully satisfy industrial demands due to the strong immiscibility and/or incompatibility. In 1990s, the ethylene–α-olefin copolymers with controllable molecular weight, molecular weight distribution and comonomer composition were commercialized by Dow Chemical and proved to be more efficient in improving the impact resistance of PP, owing to the low interfacial tension between the two components [12–18]. However, the compatibility in binary blends of PP with α-olefin copolymers has not been found to be as good as expected, determined by the primary structure and molecular composition of α-olefin copolymers.

More recently, the advent of PP in-reactor alloys or so-called in-situ blends has drawn extensive scientific and industrial interests, owing to the excellent mechanical properties and relatively low cost. A typical PP in-reactor alloy is prepared by sequential homopolymerization of propylene with Ziegler–Natta catalyst and subsequent copolymerization of propylene and α-olefins with Ziegler–Natta or metallocene catalyst [19–26]. Integrated utilization of various characterizations gives us a clear insight into the composition and structure of these alloys [27–35]. For instance, polypropylene/poly(ethylene-*co*-propylene) (PP/EPR) in-reactor alloys are mainly composed of PP, EPR, ethylene–propylene segmented copolymer (EPS) with long ethylene or propylene sequences, and possible existence of PE. Such alloys generally show complicated

* Corresponding author. Tel.: +86 10 82618533; fax: +86 10 82612857.
E-mail address: djwang@iccas.ac.cn (D. Wang).

0032-3861/$ – see front matter © 2009 Elsevier Ltd. All rights reserved.
doi:10.1016/j.polymer.2009.09.026

microstructure and typical heterophasic morphology. The EPS copolymer, acting as a compatibilizer between the dispersed EPR rubbery phase and the semicrystalline PP phase, contributes to the homogeneous dispersion of EPR spherical domains in PP matrix. The macroscopically homogeneous but microscopically separated phase structure offers PP in-reactor alloys excellent impact resistance.

In practical applications, PP in-reactor alloys can be used as structural materials independently as well as impact modifier to toughen PP. Although the compositional heterogeneity, the multi-scaled structure, and the structure-property relationship of a single alloy have been extensively investigated [24,26,36–38], little work has been reported on the polymer blending system of PP in-reactor alloys toughening PP. Therefore, in the present work, we performed systematic investigation on a series of PP blends toughened with PP/EPR in-reactor alloy, including the inter-compositional interaction, the crystalline structure, and the phase morphology as well as their influences on the mechanical properties, aiming to establish the correlation between morphological structure and mechanical properties, especially the compositional and morphological influence on impact toughness. Based on the experimental observations, schematic illustration has been proposed for structural development of the blends during impact test to elucidate the correlation between morphological structure and final mechanical properties.

2. Experimental

2.1. Materials and blends preparation

Neat polypropylene used in present study was prepared by chemical degradation of a commercial PP brand S1003, supplied by SinoPec Beijing Yansan Petrochemical Co., Ltd. The melt flow rate (MFR) of the neat PP was measured as 8.5 g/10 min (2.16 kg, 230 °C). The PP/EPR in-reactor alloy (EP-P) is a commercial product produced by Basell Company using a spherical superactive $TiCl_4$/$MgCl_2$-based catalyst, composed of 59 wt% EPR, 23 wt% PP and EPS with long propylene sequence, and 15 wt% PE and EPS with long ethylene sequence. The MFR of EP-P was determined to be 2.5 g/10 min (2.16 kg, 230 °C).

Melt blending of PP/EP-P blends (95/5, 90/10, 80/20, 70/30, 60/40, 50/50, 45/55, 30/70, wt%) was performed with a co-rotating twin screw extruder (TSE-30A). Neat PP and EP-P were also extruded for control experiment. The diameter of the screw is 30 mm and the length-to-diameter ratio is 40/1. Temperatures along the barrel were 200, 210, 220, 230, 230, 230, 230, 220, 200 and 185 °C in sequence. The screw rotating and feeding speeds were set as 250 and 25 rpm, respectively.

2.2. Differential scanning calorimetry (DSC) and successive self-nucleation and annealing (SSA)

DSC and SSA measurements were conducted under nitrogen atmosphere with a Perkin–Elmer differential scanning calorimeter (DSC-7). The calibration for temperature and melting enthalpy was performed using indium as the standard. Samples ca. 3 mg were sealed in aluminum pans and used for measurements. For DSC measurement, the samples were first heated to 200 °C and held for 5 min to erase thermal history, then cooled to 30 °C and held for 5 min, and finally heated to 200 °C again. The scanning rate employed during the thermal treating process was 10 °C/min.

Thermal fractionation by SSA was carried out according to the following steps [39]:

(1) Samples were heated from 30 to 230 °C and held for 5 min, then cooled to 10 °C and held for 5 min to create a standard thermal history.
(2) SSA procedures were performed separately for PP and PE components, since the melting points of the two components show large difference. Single-step self-nucleation experiment has been done to determine the melting domains of both PP and PE components. The first self-seeding temperature (T_s) for PP components was determined to be 169 °C, while 124 °C for PE component. The fractionation time interval adopted for adjacent T_s was 5 °C, and the annealing time at each T_s was 30 min. The chosen temperature ranges were 149–169 °C for PP components and 84–124 °C for PE components, respectively. The scanning rate employed during SSA process was 20 °C/min.
(3) After completion of the fractionation process, the melting endotherms were recorded at a heating rate of 10 °C/min from 10 to 200 °C.

2.3. Dynamic mechanical analysis (DMA)

The dynamic mechanical properties were examined in dual cantilever mode using a dynamic mechanical analyzer Q800 (TA Instruments) on rectangle specimens (length 35 mm, width 12.9 mm, and thickness 3 mm). An amplitude of 25 μm selected by means of a strain sweep test was used to ensure that the experiments were conducted in the linear viscoelastic region. The dynamic storage modulus E', the loss modulus E'' and the tangent of loss angle tan δ ($=E''/E'$) were measured between −140 and 125 °C at a constant frequency of 1 Hz and a heating rate of 3 °C/min.

2.4. Polarized optical microscopy (POM)

POM observations were carried out using an Olympus BX51 optical microscope equipped with a Linkam THMS 600 hot stage to monitor the temperature. The films with thickness of ca. 20 μm were sandwiched between two microscope cover glasses, then melted at 200 °C for 10 min to erase thermal history, and finally cooled to 130 °C at a rate of 100 °C/min for isothermal crystallization. All the polarized optical micrographs were in-situ taken using the Image-Pro Plus 5.1 software under crossed polarized light with the polarization direction horizontal.

2.5. Scanning electron microscopy (SEM)

PP/EP-P blends were cryogenically fractured in liquid nitrogen and etched in xylene for 48 h at 25 °C to remove the randomly dispersed phase. The impact fractured surfaces of notched Izod specimens were also etched under the same condition. Both the cryogenically fractured and impact fractured surfaces of PP/EP-P blends were observed with a scanning electron microscope (JEOL JSM-6700F) at an acceleration voltage of 5 kV. The surfaces of all the samples were coated with a conductive platinum layer before observation.

2.6. Measurement of mechanical properties

The tensile stress at yield and flexural modulus were measured at room temperature using an Instron 3365 universal materials testing machine, according to ASTM D638 and ASTM D790, respectively. The crosshead speed was set at 50 and 2 mm/min for tensile and flexural tests, respectively. The span for flexural test was 40 mm. The reported values of the mechanical properties were averaged at six independent measurements.

The notched Izod impact strength was measured on a Ceast pendulum impact strength tester CSI-137C at room temperature, according to ASTM D256. The drop velocity was 3.5 m/s and the testing results were the average of ten parallel experiments.

All the specimens for mechanical tests were prepared by injection molding at 210 °C.

3. Results and discussion

3.1. Inter-compositional interactions between EP-P and neat PP

3.1.1. Inter-compositional interaction in crystalline region

The crystallization and melting temperatures of PP and PE components in PP/EP-P blends are summarized in Table 1. These data are helpful for understanding the interaction/miscibility of EP-P components with neat PP, particularly in crystalline region. The PP component in PP/EP-P blends constituted by PP from EP-P and neat PP shows a single crystallization temperature (T_c) and a single melting temperature (T_m). This fact reveals that the PP component from EP-P is thoroughly miscible with neat PP to form co-crystals during crystallization. On the other hand, two well-separated melting peaks corresponding to PP and PE components can be observed. The value of T_{mPP} decreases very slightly with the increase of EP-P content, while that of T_{mPE} remains almost constant. Such tiny decrease of T_{mPP} may be due to the partial miscibility of PP and EPS copolymers. The crystallizable PP sequences in EPS copolymers are considered to be capable of participating in the crystallization process of PP and disturbing the perfection of PP crystals to some extent. This also indicates that the blending of EP-P with neat PP little affects the fine structure of PP and PE crystals and in particular the lamellae thickness, which will be further proved by SSA results. As shown in Table 1, T_{cPP} decreases with the addition of EP-P, while T_{cPE} increases. As a result, the value of $T_{cPP} - T_{cPE}$ becomes smaller for PP/EP-P blends with higher EP-P content (Fig. 1). We suggest that the variation of T_c values results from the mutual interferences between PP and the heterogenous components such as EPS and EPR copolymers. The insertion of crystallizable PP sequences from EPS copolymers into PP crystallization together with the effective diluting effect from the rest portions of EPS copolymers and the molten EPR molecules slow down the diffusion of PP chains, suppress its ordered arrangement, and eventually delay the nucleation. At the same time, the nucleation and growth of PE crystals may also be postponed by the existing PP crystals, since the crystallization of PP component takes place prior to the crystallization of PE component.

SSA is essentially a thermal fractionation method based on the sequential application of self-nucleation and annealing steps on polymer samples, giving useful information on the distribution of short chain branching and lamellar thickness. SSA technique has been adopted by Müller to evaluate the miscibility of LLDPE/HDPE and ULDPE/HDPE [39]. The co-crystallization effect (miscibility)

Table 1
Crystallization and melting temperatures of PP and PE components.

PP/EP-P	T_c (°C)		T_m (°C)	
	PP component	PE component	PP component	PE component
100/0	118.2	–	161.8	–
95/5	117.2	–	161.7	–
90/10	117.1	95.2	161.4	119.4
80/20	116.9	95.9	161.5	118.5
70/30	117.7	97.6	160.9	117.8
60/40	117.2	100.9	161.2	118.3
50/50	117.1	102.1	161.2	118.3
45/55	116.4	101.6	161.5	118.5
40/60	116.3	101.7	161.0	118.3
30/70	116.4	101.9	160.5	118.0
0/100	115.7	102.1	160.0	117.6

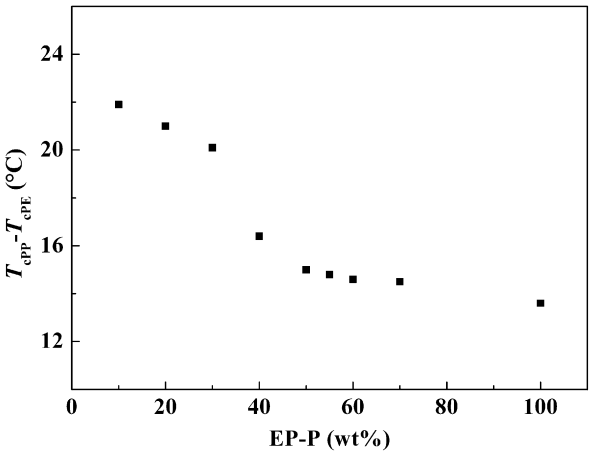

Fig. 1. Variation of $T_{cPP} - T_{cPE}$ with EP-P content.

was interpreted by how the number of thermal fractions generated by SSA in the blends varies with composition and by comparing the relative amounts of the thermal fractions.

Fig. 2a shows the melting endotherms of PP component in PP/EP-P blends after a five-step SSA treatment at 169, 164, 159, 154, and 149 °C. Since the first self-seeding temperature does not cause any annealing or lamellae thickening, only four steps are

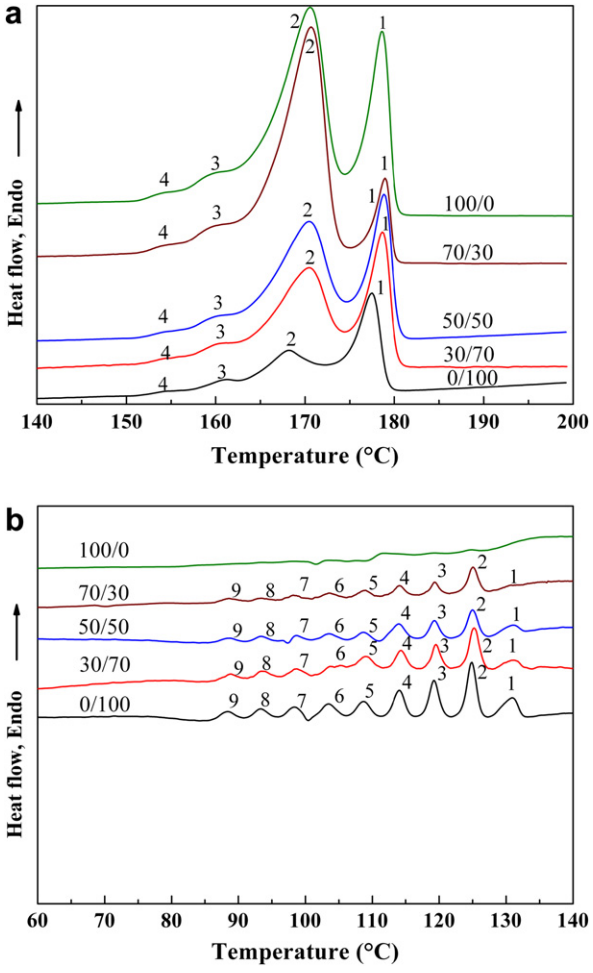

Fig. 2. DSC endotherms of PP (a) and PE (b) components after SSA treatment.

Table 2
Melting temperatures of PP component after SSA treatment.

PP/EP-P	T_m (°C)			
	1	2	3	4
100/0	178.8	170.5	160.5	154.5
70/30	178.9	170.6	160.4	154.8
50/50	178.8	170.4	160.3	154.6
30/70	178.6	170.6	160.4	154.8
0/100	177.5	168.5	161.3	154.7

able to produce annealing. Each fusion endotherm corresponds to the melting of a particular lamellar population made up of the linear sections of the chains with similar short chain branching and distribution, while neat PP is supposed to be fractionated by molecular weight in view of its negligible branching content. The melting temperatures of PP fractions corresponding to the annealing steps are shown in Table 2. It can be observed that the T_ms, for the groups of crystals in neat EP-P annealed at 164 and 159 °C, are a little lower than that in neat PP and PP/EP-P blends, which may be attributed to the thinner lamellae caused by chain branching and defects. Also, the T_ms for the rest groups of lamellae are situated at similar positions, irrespective of the blends composition. Such behavior confirms the occurrence of co-crystallization and thorough miscibility of PP component from EP-P and neat PP, as DSC illustrates. In addition, a better molecular segregation and thermal fractionation between PP and PE components also took place during SSA treatment. As shown in Fig. 2b, the number of PE fractions after SSA treatment is equal in neat EP-P and all the PP/EP-P blends, and the corresponding T_ms also show no significant dependence on the blends composition (Table 3). This reveals that the PE crystals, particularly at the scale of lamellae, have similar thickness in all the samples, and there is no co-crystallization effect/miscibility between PP and PE components.

3.1.2. Inter-compositional interaction in amorphous region

DMA is adopted to investigate the intermolecular interaction and phase structure in amorphous region, as this technique can make clear whether or not there exists a compatibility or non-compatibility between different components. In DMA measurement, the miscible polymer blends show a homogeneous phase at the molecular level and are characterized by a single glass transition temperature (T_g), whereas the immiscible polymer blends show two glass transition temperatures and have two or more separated phases.

The abrupt transformation of tan δ in DMA spectra represents the glass transitions corresponding to relaxations of different motion units from "frozen" state to "free". Temperature dependences of tan δ for neat PP, neat EP-P, and their blends are shown in Fig. 3. It can be observed that there are four distinct transitions ascribed to segmental relaxations of PP, EPS, EPR, and PE, respectively, in the order of decreasing temperature. The T_g of EPS copolymers appears at about −30 °C with low intensity and as a weak shoulder in the transition domain of EPR copolymers. The

Table 3
Melting temperatures of PE component after SSA treatment.

PP/EP-P	T_m (°C)								
	1	2	3	4	5	6	7	8	9
70/30	–	125.1	119.4	114.3	108.9	103.6	98.5	93.7	88.7
50/50	131.3	125.1	119.4	114.2	108.7	103.5	98.8	93.5	88.6
30/70	131.1	125.1	119.5	114.4	108.9	103.6	98.5	93.7	89.0
0/100	131.2	124.9	119.4	114.2	108.8	103.5	98.3	93.5	88.5

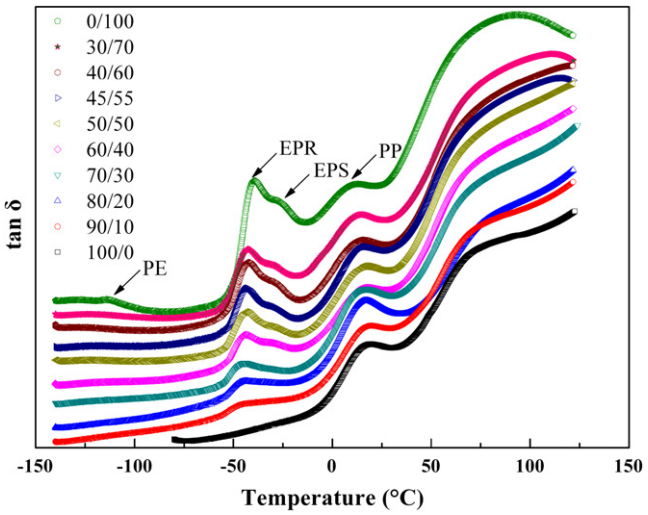

Fig. 3. Temperature dependence of loss angle tangent tan δ.

value of $T_{g,EPS}$ matches the T_g of typical linear low-density PE (LLDPE), i.e. the EPS copolymers can be considered as a kind of LLDPE. The loss intensities of both EPR and EPS copolymers rise gradually with the increase of EP-P content, while that of PP decreases. At the same time, it can be found that the T_gs of EPR and EPS copolymers shift to higher temperatures, while the T_g of PP shifts to lower temperature. The transition peaks of EPR, EPS, and PP are inclined to form a broad loss peak. Such variation of T_gs with EP-P content for PP, EPS, and EPR, as summarized in Fig. 4, suggests the existence of inter-compositional interaction in amorphous region, in which the EPS copolymers play an important role. As discussed above that the crystallizable PP sequences in EPS chains were incorporated into the lattice of PP crystals, while the rest portions were excluded into the amorphous interlamellar regions, this enhanced the mutual incorporation and efficient diffusion of the amorphous PP segments and EPR molecules. The motion of the amorphous PP segments was strengthened by the "softening" effect from more flexible EPR molecules. In contrast, the motion of EPR and EPS components was weakened by the "inhibiting" effect from rigid PP segments. Such inter-compositional interaction lowers the T_g of PP, while enhances the T_gs of EPR and EPS copolymers (Fig. 4), and becomes more pronounced with the addition of EP-P content.

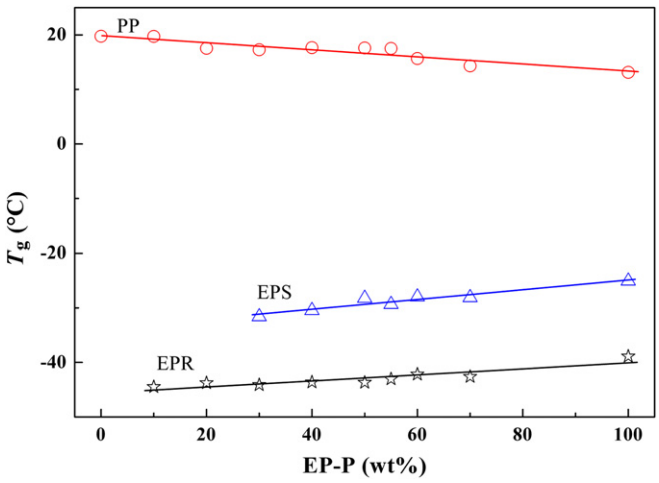

Fig. 4. Influence of EP-P content on glass transition temperatures of PP, EPR and EPS.

3.2. Optical microscopic observation on crystalline structure of PP/EP-P blends

The crystalline structure of the PP/EP-P blends after isothermal crystallization at 130 °C is shown in Fig. 5. Neat PP crystallizes in the form of well-defined and perfect spherulites, and the spherulites impinge on each other forming polygonal structure with apparent boundaries. Such crystallization morphology endows neat PP with excellent rigidity. However, the concentrated stress in the sharp interspherulitic boundaries weakens the impact resistance. It can be noted that EP-P content markedly influences the structure of PP crystals in the PP/EP-P blends. The spherulites structure suffers deterioration with the addition of EP-P, and the average size of the crystalline domains becomes smaller. In PP/EP-P blends with lower EP-P content (e.g. 30 wt%), the molten EPR droplets are homogeneously dispersed in PP spherulites and interspherulitic regions. The spherulites diffuse into each other and the interspherulitic boundaries get blurred, with respect to that of neat PP. Furthermore, no spherulites with distinguishable Maltese-crosses can be discerned in the blends with higher EP-P content (e.g. 70 wt%) and particularly in neat EP-P. The crystalline structure seems more irregular and randomly scattered, and the interspherulitic boundaries completely disappear. The evolution of crystalline structure with EP-P content can be considered as a "Grain Refinement" process, which is advantageous to eliminate stress concentration. It's also the synergic effect that the insertion of crystallizable PP sequences from EPS copolymers into PP crystals and the diluting effect of the rest portions from EPS copolymers and EPR molecules, hinders the formation of regular spherulites, and reduces the size of crystal domains.

3.3. Morphology investigation on PP/EP-P blends by SEM

For polymer blends, the size and size distribution of dispersed phase as well as the interfacial structure play important roles in determining the ultimate mechanical properties. Therefore, it is essential to fully understand the phase morphology of PP/EP-P blends and its correlation with mechanical properties. As shown in Fig. 6, the fractured surface of neat EP-P before xylene etching appears smooth and homogeneous, implying that there exists good adhesion between the different phases, and typical co-continuous structure can be clearly observed after xylene etching. Such phase

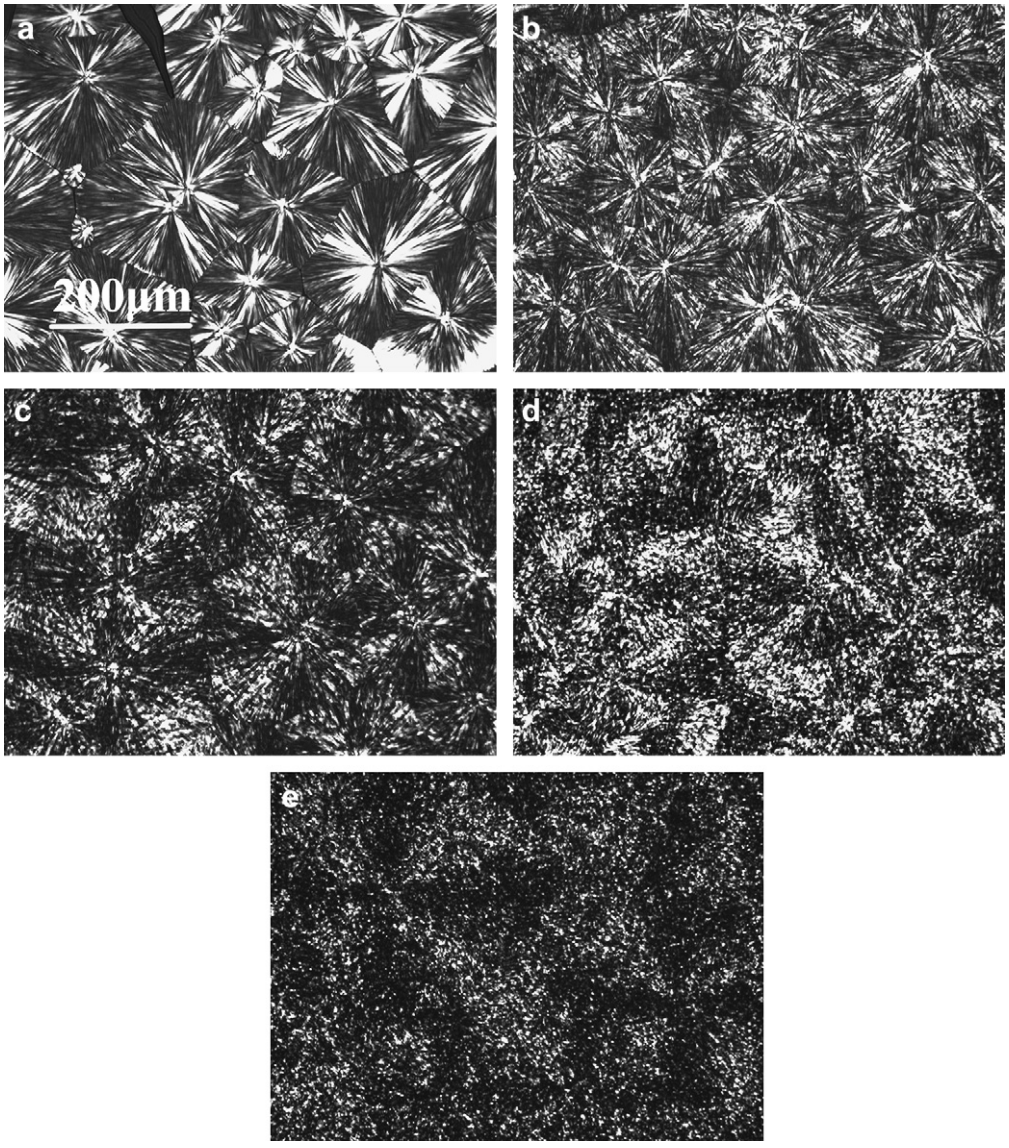

Fig. 5. POM micrographs after isothermal crystallization at 130 °C: (a) neat PP; (b) PP/EP-P (70/30); (c) PP/EP-P (50/50); (d) PP/EP-P (30/70); (e) neat EP-P.

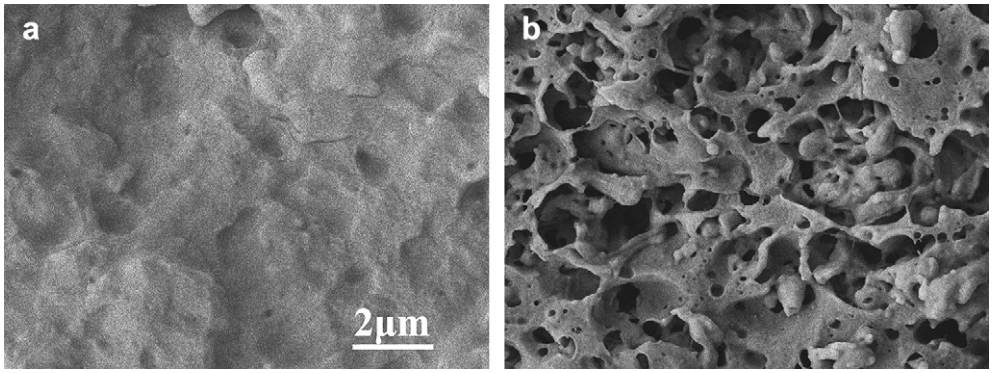

Fig. 6. SEM micrographs of cryogenically fractured surface of neat EP-P: (a) before xylene etching; (b) after xylene etching.

structure together with good adhesion guarantee neat EP-P with excellent impact resistance. Fig. 7 showed that PP/EP-P blends exhibit characteristic "sea–island" structure, where the "islands" are homogenously dispersed in the "sea", differing from the co-continuous structure of neat EP-P. Apparently, the "sea" and "island" are attributed to the PP matrix and the EPR rubbery phase, respectively. Increasing EP-P content has no evident influence on the size and size distribution of the rubbery particles, whereas increases the number of the rubbery particles and thus leads to decrease of interparticle distance. In contrast, in the traditional

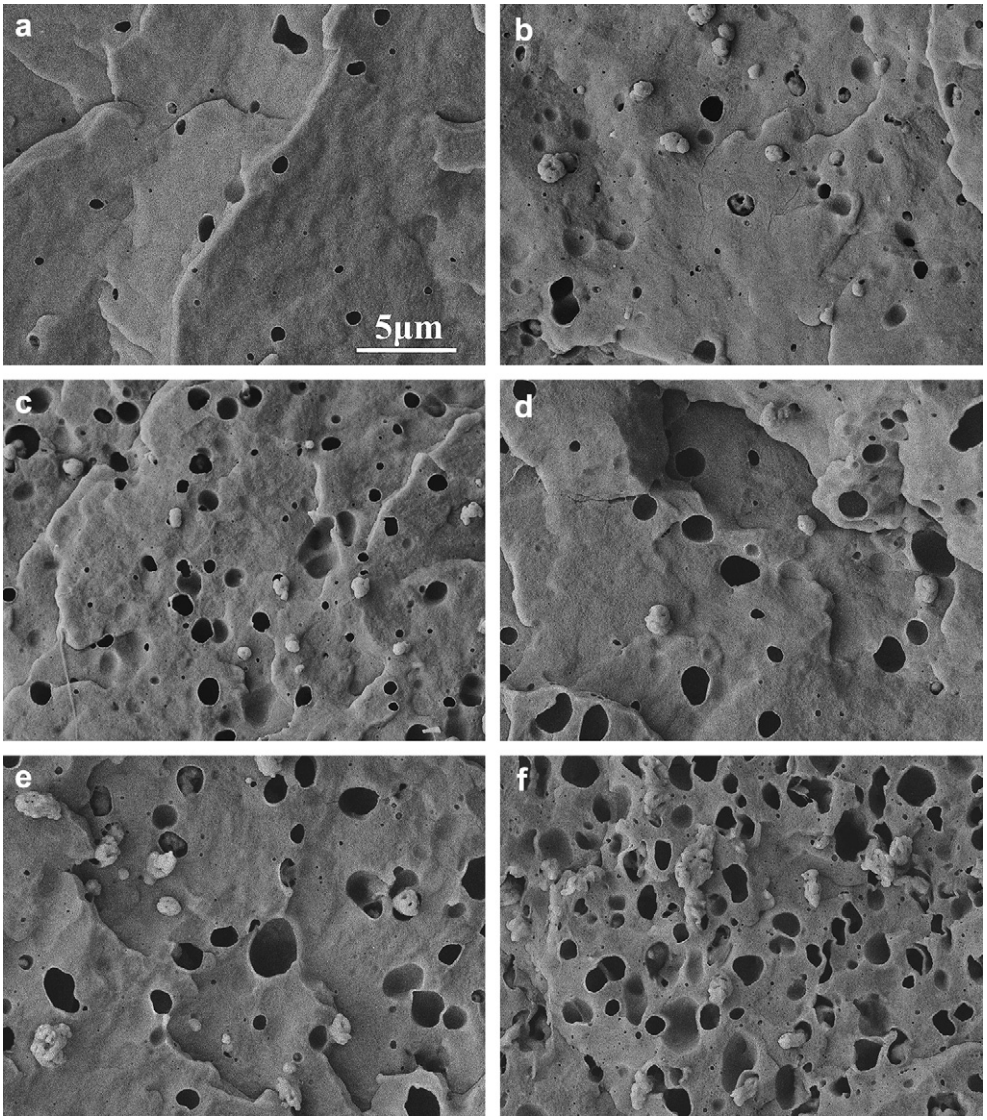

Fig. 7. SEM micrographs of cryogenically fractured surfaces of PP/EP-P blends after xylene etching: (a) PP/EP-P (95/5); (b) PP/EP-P (80/20); (c) PP/EP-P (70/30); (d) PP/EP-P (60/40); (e) PP/EP-P (50/50); (f) PP/EP-P (30/70).

PP/EPDM blends, the size, size distribution, and the number of the rubbery particles are all remarkably dependent on the EPDM content [8]. Therefore, it can be speculated that, besides EP-P content, some more complex factors should be taken into account to interpret the morphology evolution of the PP/EP-P blends.

As well known, Taylor has suggested several equations considering viscosity ratio, shear stress, droplet diameter, and interfacial tension as main factors to investigate dispersed particles deformation and breakup for Newtonian systems in shear flow fields [40–42]. Later on, Van Oene successfully applied Taylor's equations to polymer blends, and demonstrated that the elastic contribution to the interfacial tension can result in the tendency for a phase of high elasticity to encapsulate the one of low elasticity [43]. The parameters including shear rate, viscosity and elasticity ratios, interfacial tension, and blends composition, would play important roles in controlling deformation and disintegration of dispersed phase during polymer blends processing. Since all the PP/EP-P blends experienced the same processing condition, the influence of shear rate on phase morphology is not our concern. In addition, the dispersed EPR phase can be easily engulfed in PP matrix in terms of their respective elasticity. Herein, we would concentrate on the influence of viscosity ratio, interfacial tension, and blends composition.

Extraction of neat EP-P by boiling *n*-hexane has been performed to obtain separated fractions so as to calculate the viscosity ratio of dispersed phase to matrix. The soluble fraction in boiling *n*-hexane is approximately ascribed to the dispersed EPR phase, and the insoluble fraction is ascribed to the PP component in EP-P. The viscosity values of neat PP and EP-P fractions recorded during MFR measurement are summarized in Table 4. As the PP matrix made up of neat PP and PP from EP-P, it can be deduced rationally that the viscosity of the PP matrix lies between 0.5 and 3.0 E3 Pa.s. Considering that the dispersed phase exhibits higher viscosity (3.5 E3 Pa.s) than PP matrix, the viscosity ratio should be always above unity. Moreover, with the addition of EP-P, the viscosity of PP matrix increases with the relative content of PP from EP-P in PP matrix, and consequently the viscosity ratio would become smaller and closer to unity, which is beneficial to reduce the size and size distribution of the dispersed particles [44–47]. On the other hand, the compatibilization effect of EPS copolymers reduces the interfacial tension between PP matrix and EPR dispersed phase, thus limiting the enlargement of dispersed particles size and broadening of size distribution, and this effect becomes more remarkable with the increase of EPS content in PP/EP-P blends at higher EP-P content. The evolution of viscosity ratio and interfacial tension with the addition of EP-P is favorable for the homogeneous dispersion of rubbery particles. Nevertheless, the EP-P content has positive effect on enlarging the dispersed particles size and broadening its distribution [45,48]. Therefore, it's the synergic effect of viscosity ratio, interfacial tension, as well as blends composition that determines the ultimate phase morphology.

3.4. Correlation between morphological structure and mechanical properties

The mechanical properties of PP/EP-P blends are shown in Fig. 8. Neat PP exhibits the poorest impact strength (2.3 kJ/m^2) and the best rigidity, whereas neat EP-P behaves adversely. The impact strength increases with the addition of EP-P, however, the tensile stress at yield and the flexural modulus all decrease. The brittle–ductile transition occurs at EP-P content about 40 wt%, as the impact strength at this point rises abruptly. The specimens with EP-P content exceeding 40 wt% and neat EP-P could not be broken under the same testing condition due to their good impact toughness.

Table 4
Viscosity of components in PP/EP-P blends.

Samples	Neat PP	PP from EP-P	Dispersed phase
Viscosity (E3 Pa.s)	0.5	3.0	3.5

Fractographic observation on the impact fractured surface can provide useful information concerning deformation behaviors of the PP/EP-P blends. SEM micrographs of the impact fractured surfaces after xylene etching are shown in Fig. 9. The white arrows indicate the crack-propagation direction. The fractured surface of neat PP is smooth (Fig. 9a), resulting from the unstable crack-propagation and the brittle failure, which is consistent with its poor

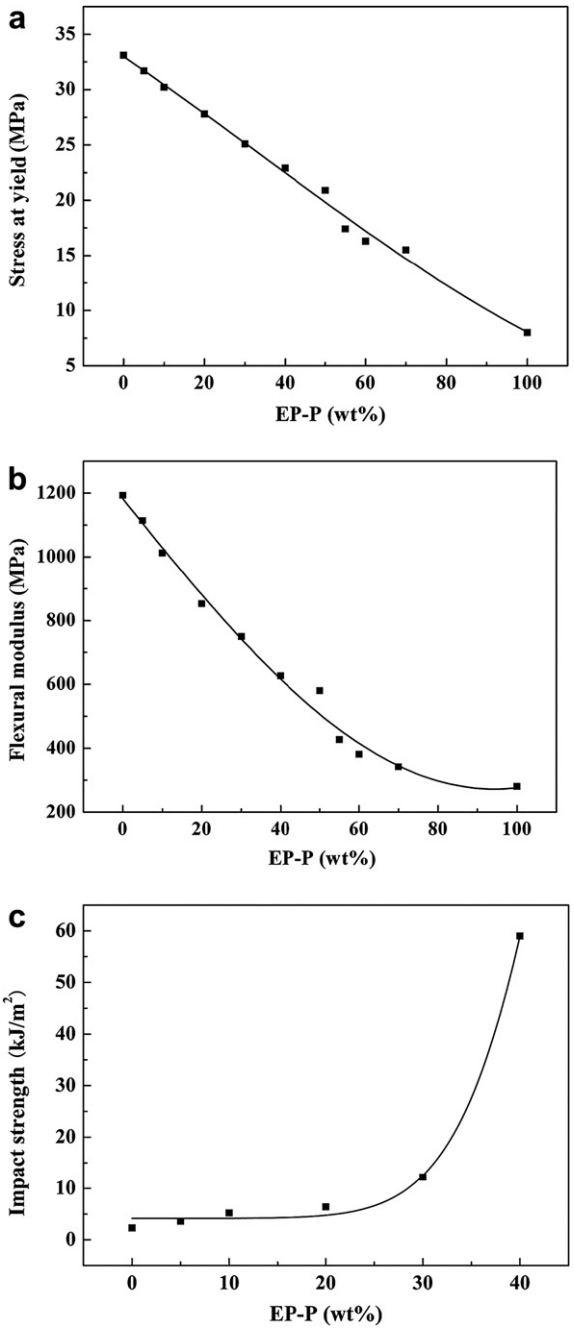

Fig. 8. Variations of mechanical properties with EP-P content: (a) stress at yield; (b) flexural modulus; (c) impact strength.

impact resistance. The incorporation of EP-P would contribute to the enhancement of impact resistance. As shown in Fig. 9b–d, good adhesion can be observed between the PP matrix and the rubbery particles, manifesting with the appearance of PP fibrils at the interphases of PP matrix and rubbery particles, which have been also found in a single PP in-reactor alloy [36,49]. Such fibrous linking seems to be caused by the mergence and rearrangement of PP segments locating at the interphases. During impact test, the PP segments may be drawn out to form the fibril-like structure, which helps to improve the impact resistance. However, these blends with EP-P content no more than 30 wt% still break in brittle fashion (Fig. 9b–d). In contrast, the blends with EP-P content more than 30 wt% break in ductile fashion (Fig. 9e and f). Strip-like protrusions can be observed on the fractured surfaces along the crack-propagation direction, and many fine and regular pleats exist between the protrusions. It is obvious that shear deformation and shear yielding are the primary toughening mechanism for these blends. Moreover, there are no discernable cavities and crazes on the surfaces, implying the existence of high cavitation stress and strong interfacial adhesion. Under impact, the rubbery particles firstly elongate along the external stress direction, then the overlap of the adjacent stress fields surrounding the rubbery particles induces shear yielding of PP matrix, and subsequently the PP matrix deforms as an entire with the rubbery phase. The cooperative motion of PP matrix and rubbery phase consumes large amounts of energy, and hinders the initiation and propagation of micro-cracks.

Based on the observations in Fig. 9, we herein attempt to summarize the compositional and morphological influences on the mechanical properties of PP/EP-P blends, in particular the impact strength. Schematic illustration has been proposed for the structural development of neat PP (Fig. 10a_1–a_3), PP/EP-P blends (Fig. 10b_1–b_3 and c_1–c_3), and neat EP-P (Fig. 10d_1–d_3) during impact test. Neat PP exhibits excellent rigidity because of the perfect spherulites (Fig. 10a_1), however, brittle fracture would take place immediately on suffering external stress due to the stress concentration in the interspherulitic boundaries (Fig. 10a_2 and a_3). On adding EP-P, the mobility of PP chains would be promoted by the "softening" effect from EPR molecules, and the EPS copolymers can act as tie molecules linking adjacent lamellae of PP crystals, which facilitate the enhancement of impact toughness. In the case of

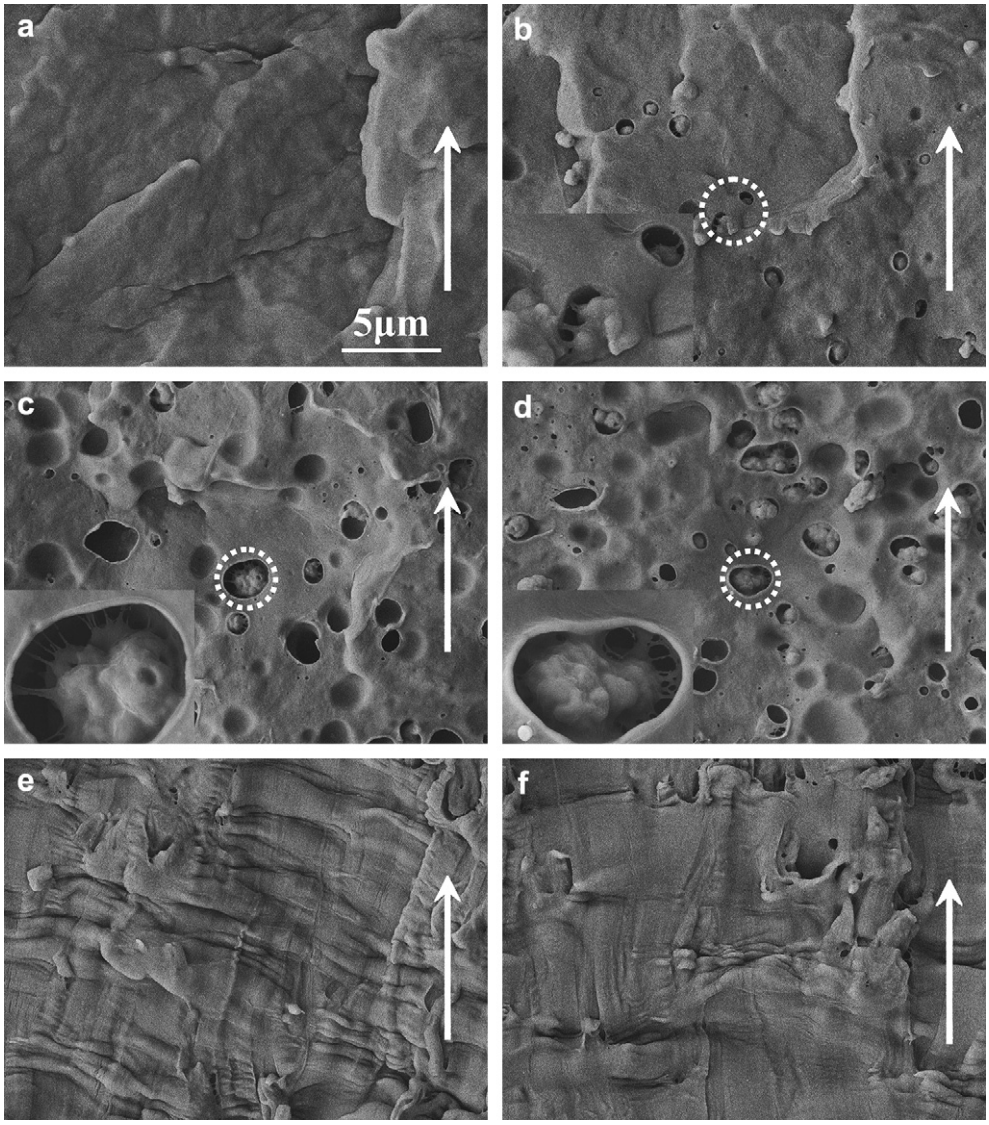

Fig. 9. SEM micrographs of the impact fractured surfaces after xylene etching: (a) neat PP; (b) PP/EP-P (95/5); (c) PP/EP-P (80/20); (d) PP/EP-P (70/30); (e) PP/EP-P (60/40); (f) PP/EP-P (50/50). The insets are the high-magnification images of the PP fibrils connecting the EPR rubbery particles and the PP matrix in the white circles. The arrow indicates the crack-propagation direction.

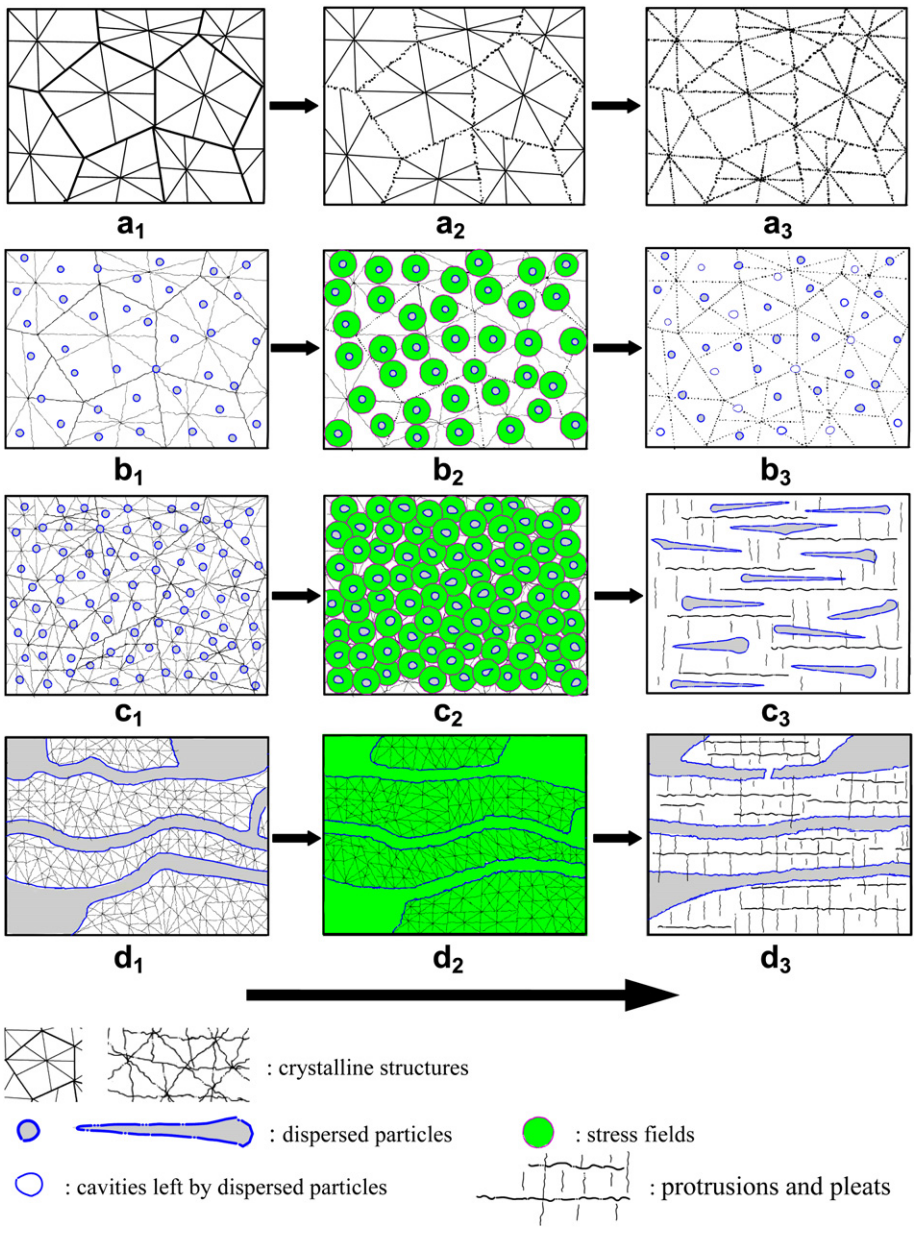

Fig. 10. Schematic illustration for structural development of neat PP (a_1–a_3), PP/EP-P blends (EP-P content $\leq$30 wt%, b_1–b_3; and EP-P content >30 wt%, c_1–c_3), and neat EP-P (d_1–d_3) during impact test. The graphs from the left column to the right represent the initial, the intermediate, and the ultimate states during impact test. The arrow at the bottom indicates the impact direction.

PP/EP-P blends with EP-P content no more than 30 wt%, despite the diffusion of PP spherulites and the blurring of interspherulitic boundaries (Fig. 10b_1), there still remains some stress concentration in the interspherulitic boundaries. Besides this, the stress field around a rubbery particle is slightly affected by the presence of other particles, and is simply a superposition of those around isolated particles, as the particles are greatly separated in PP matrix (Fig. 10b_2). Such crystalline structure and phase morphology result in the ultimate brittle failure of these blends (Fig. 10b_3). Otherwise, the stress field in blends with EP-P content more than 30 wt% is no longer a simple superposition. The stress fields around neighboring particles would overlap and interact with each other owing to the decreased interparticle distance (Fig. 10c_2), promoting the generation of shear yielding and plastic deformation of PP matrix (Fig. 10c_3). In addition, PP crystals in these blends seem rather irregular and randomly scattered, and it's difficult for such crystalline structure to form stress concentration. As a result, a transition to ductile behavior occurs for these blends. As far as neat EP-P is concerned, the stress field produced by the motion of rubbery phase is widespread in the bulk due to the co-continuous phase structure (Fig. 10d_1 and d_2), which together with the more scattered crystalline structure enables neat EP-P to possess the optimal impact toughness.

4. Conclusions

In the present study, the polymer blending system of EP-P in-reactor alloy toughening PP was systematically investigated. It has been found that there exist some intermolecular interactions between EP-P components and neat PP. The PP component from EP-P can be completely miscible with the neat PP, and they together serve as the matrix of the PP/EP-P blends, while the EPR copolymers act as the dispersed phase. The compatibilization effect of EPS copolymers improves the compatibility between EPR dispersed

phase and PP matrix, strengthening mutual incorporation and effective diffusion of the amorphous PP segments and EPR molecules. In addition, the EP-P content markedly influences the crystalline structure and phase morphology of the PP/EP-P blends. The PP spherulites undergo deterioration with the addition of EP-P, and consequently become highly irregular and randomly scattered. In contrast, the homogeneous phase morphology can be maintained that the size and size distribution of the rubbery particles remain invariant, and only the interparticle distance is reduced. Such evolution of crystalline structure and phase morphology with the addition of EP-P is favorable for the enhancement of impact resistance. Schematic illustration has been proposed for structural development of the PP/EP-P blends during impact test, to elucidate the compositional and morphological influence on mechanical properties.

Acknowledgement

This work was supported by the National High Technology Research and Development Program of China (2007AA03Z554).

References

[1] Danesi S, Porter RS. Polymer 1978;19:448.
[2] Greco R, Mancarella C, Martuscelli E, Ragosta G, Yin J. Polymer 1987;28:1929.
[3] D'Orazio L, Mancarella C, Martuscelli E, Polato F. Polymer 1991;32:1186.
[4] Nitta K, Kawada T, Yamahiro M, Mori H, Terano M. Polymer 2000;41:6765.
[5] Pukánszky B, Tüdös F, Kalló A, Bodor G. Polymer 1989;30:1399.
[6] Karger-Kocsis J, Kalló A, Kuleznev VN. Polymer 1984;25:279.
[7] van der Wal A, Mulder JJ, Oderkerk J, Gaymans RJ. Polymer 1998;39:6781.
[8] van der Wal A, Nijhof R, Gaymans RJ. Polymer 1999;40:6031.
[9] (a) Gupta AK, Purwar SN. Journal of Applied Polymer Science 1984;29:1079; (b) Gupta AK, Purwar SN. Journal of Applied Polymer Science 1984;29:1595; (c) Gupta AK, Purwar SN. Journal of Applied Polymer Science 1984;29:3513; (d) Gupta AK, Purwar SN. Journal of Applied Polymer Science 1985;30:1777; (e) Gupta AK, Purwar SN. Journal of Applied Polymer Science 1985;30:1799; (f) Gupta AK, Purwar SN. Journal of Applied Polymer Science 1986;31:535.
[10] Thanyaprueksanon S, Thongyai S, Praserthdam P. Journal of Applied Polymer Science 2007;103:3609.
[11] Liang JZ, Li RKY. Journal of Applied Polymer Science 2000;77:409.
[12] Yamaguchi M, Miyata H. Macromolecules 1999;32:5911.
[13] Prieto Ó, Pereña JM, Benavente R, Cerrada ML, Pérez E. Macromolecular Chemistry and Physics 2002;203:1844.
[14] Bensason S, Minick J, Moet A, Chum S, Hiltner A, Baer E. Journal of Polymer Science Part B Polymer Physics 1996;34:1301.
[15] Bensason S, Nazarenko S, Chum S, Hiltner A, Baer E. Polymer 1997;38:3913.
[16] McNally T, McShane P, Nally GM, Murphy WR, Cook M, Miller A. Polymer 2002;43:3785.
[17] Da Silva ALN, Tavares MIB, Politano DP, Coutinho FMB, Rocha MCG. Journal of Applied Polymer Science 1997;66:2005.
[18] Thomas CY. Polymer Engineering and Science 2001;41:656.
[19] Cecchin G, Morini G, Pelliconi A. Macromolecular Symposia 2001;173:195.
[20] Galli P. Progress in Polymer Science 1994;19:959.
[21] Galli P, Vecellio G. Progress in Polymer Science 2001;26:1287.
[22] Liu JG, Dong JY, Cui NN, Hu YL. Macromolecules 2004;37:6275.
[23] Pires M, Mauler RS, Liberman SA. Journal of Applied Polymer Science 2004; 92:2155.
[24] Fan ZQ, Zhang YQ, Xu JT, Wang HT, Feng LX. Polymer 2001;42:5559.
[25] Randall JC. Journal of Polymer Science Part A Polymer Chemistry 1998;36: 1527.
[26] Fu ZS, Fan ZQ, Zhang YQ, Feng LX. European Polymer Journal 2003;39:795.
[27] Cai HJ, Luo XL, Ma DZ, Wang JM, Tan HS. Journal of Applied Polymer Science 1999;71:93.
[28] Feng Y, Hay JN. Polymer 1998;39:6723.
[29] Mirabella JFM. Polymer 1993;34:1729.
[30] Zacur R, Goizueta G, Clapiati N. Polymer Engineering and Science 1999;39:921.
[31] Chen Y, Chen Y, Chen W, Yang DC. Polymer 2006;47:6808.
[32] Cai HJ, Luo XL, Chen XX, Ma DZ, Wang JM, Tan HS. Journal of Applied Polymer Science 1999;71:103.
[33] Lin ZH, Peng M, Zheng Q. Journal of Applied Polymer Science 2004;93:877.
[34] Xu JT, Fu ZS, Wang XP, Geng JS, Fan ZQ. Journal of Applied Polymer Science 2005;98:632.
[35] Galli P, Collina G, Sgarzi P, Baruzzi G, Marchetti E. Journal of Applied Polymer Science 1997;66:1831.
[36] Zhu HJ, Monrabal B, Han CC, Wang DJ. Macromolecules 2008;41:826.
[37] Starke JU, Michler GH, Grellmann W, Seidler S, Gahleitner M, Fiebig J, et al. Polymer 1998;39:75.
[38] Doshev P, Lach R, Lohse G, Heuvelsland A, Grellmann W, Radusch HJ. Polymer 2005;46:9411.
[39] Arnal ML, Sánchez JJ, Müller AJ. Polymer 2001;42:6877.
[40] Taylor GI. Containing Papers of a Mathematical and Physical Character (1905–1934). Proceedings of the Royal Society of London. Series A 1932;138:41.
[41] Taylor GI. Containing Papers of a Mathematical and Physical Character (1905–1934). Proceedings of the Royal Society of London. Series A 1934;146:501.
[42] Taylor GI. Mathematical and Physical Sciences (1934–1990). Proceedings of the Royal Society of London. Series A 1954;226:34.
[43] Vanoene H. Journal of Colloid and Interface Science 1972;40:448.
[44] Utracki LA, Shi ZH. Polymer Engineering and Science 1992;32:1824.
[45] Serpe G, Jarrin J, Dawans F. Polymer Engineering and Science 1990;30:553.
[46] Favis BD, Chalifoux JP. Polymer Engineering and Science 1987;27:1591.
[47] Wu SH. Polymer Engineering and Science 1987;27:335.
[48] Favis BD, Therrien D. Polymer 1991;32:1474.
[49] Tan HS, Li L, Chen ZN, Song YH, Zheng Q. Polymer 2005;46:3522.